Biomineralization

DOI: 10.1002/anie.201406131

Selective Formation of Metastable Ferrihydrite in the Chiton Tooth**

*Lyle M. Gordon, Jessica K. Román, R. Michael Everly, Michael J. Cohen, Jonathan J. Wilker, and Derk Joester**

Abstract: *Metastable precursors are thought to play a major role in the ability of organisms to create mineralized tissues. Of particular interest are the hard and abrasion-resistant teeth formed by chitons, a class of rock-grazing mollusks. The formation of chiton teeth relies on the precipitation of metastable ferrihydrite (Fh) in an organic scaffold as a precursor to magnetite. In vitro synthesis of Fh under physiological conditions has been challenging. Using a combination of X-ray absorption and electron paramagnetic resonance spectroscopy, we show that, prior to Fh formation in the chiton tooth, iron ions are complexed by the organic matrix. In vitro experiments demonstrate that such complexes facilitate the formation of Fh under physiological conditions. These results indicate that acidic molecules may be integral to controlling Fh formation in the chiton tooth. This biological approach to polymorph selection is not limited to specialized proteins and can be expropriated using simple chemistry.*

The chiton radula is a ribbon-like rasping tongue with many rows of extremely hard, wear-resistant, and self-sharpening teeth designed to withstand the stresses of grazing on rocks.[1] These remarkable properties result from the incorporation of nanocrystalline magnetite (Fe_3O_4) in a nanofibrous chitin scaffold of surprising chemical and structural complexity.[2] However, magnetite is not formed directly from solution. Instead, mineralization commences with the formation of metastable ferrihydrite (Fh). Fh transforms into magnetite in a second step, presumably by a reductive transformation.[3] The chiton has mastered the structural polymorphism of iron oxides and their complex chemistry, which has been difficult to reproduce in the laboratory, particularly under mild conditions. Controlling and understanding the mechanisms governing phase transformations of iron oxides, in particular Fh, is also of great importance for industrial applications, environmental science, and geology.[4] The recent emergence of non-classical nucleation and particle-mediated growth for iron oxides illustrates that our understanding of the chemistry and phase transformations of iron oxides still has significant gaps.[5]

The study of iron-mineralizing organisms has been a powerful approach to gain mechanistic insight and develop bioinspired routes to synthetic materials.[1a,6] The chiton is a model system for extracellular, matrix-mediated iron oxide biomineralization.[7] Newly formed rows of teeth move along the radula to replace worn ones every few days, as if on a conveyor belt. Therefore, all stages of tooth development and the associated mineral phases can be simultaneously observed in one animal. Developmental stages can be differentiated based on the color (Figure 1). Stage 1, 'unmineralized' teeth, are colorless and are primarily comprised of a hydrogel consisting of the polysaccharide α-chitin, proteins, and water. Stage 2 teeth are brown, containing predominantly ferrihydrite ($Fe_{8.2}O_{8.5}(OH)_{7.4}{\cdot}3H_2O$).[3b,5a,8] In stage 3, transformation of Fh to magnetite (Fe_3O_4) results in a gradual change from brown to black.[3b] Stage 4 teeth are completely black when the cusp reaches its final density of magnetite. In

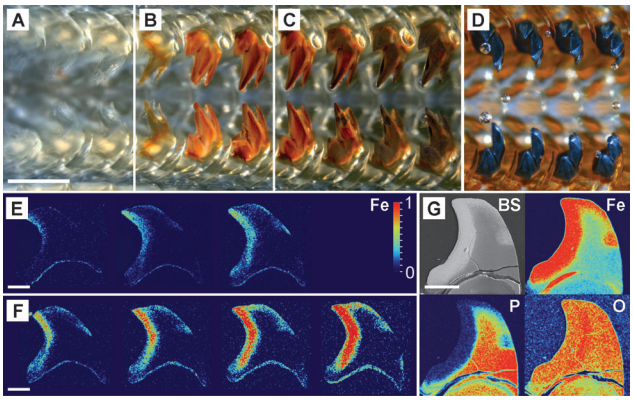

Figure 1. Stages of mineralization in *K. tunicata*. A–D) Top down view of radula with representative rows of teeth from stages 1 (A), 2 (B), 3 (C), and 4 (D). E,F) Maps of SEM-EDS-normalized iron concentrations of longitudinal sections in stages 2 (E) and 3 (F). G) BSE-SEM and SEM-EDS elemental maps of longitudinal section of stage 4 (fully mineralized tooth), showing a Fe/P/O-rich core (iron phosphate) and a Fe/O-rich cap (magnetite). Scale bars represent 500 μm in A–D and 100 μm in E–G.

[*] Dr. L. M. Gordon, M. J. Cohen, Dr. D. Joester
Department of Materials Science and Engineering
Northwestern University
2220 Campus Drive, Evanston, IL 60201 (USA)
E-mail: d-joester@northwestern.edu
J. K. Román, Dr. R. M. Everly, Dr. J. J. Wilker
Department of Chemistry, Purdue University
560 Oval Drive, West Lafayette, IN 47907 (USA)

[**] The NSF (DMR-0805313, DMR-1106208, CHE-0952928), NU-MRC (NSF-MRSEC DMR-1121262), IIN, and NSERC, supported this work in part. J.J.W. also appreciates funding from ONR (N000141310327, N000141310245). Portions of this work were performed at the NU OMM, the J. B. Cohen XRD Facility, and the NUANCE Facility. The NU-MRC (NSF-MRSEC DMR-1121262), NU-NSEC, Keck Foundation, State of Illinois, and NU supported these facilities. Further work was performed at DND-CAT located at Sector 5 of the Advanced Photon Source (APS). Use of the APS was supported by the DOE (DE-AC02-06CH11357). We thank Dr. Q. Ma for assistance with X-ray absorption spectroscopy, Prof. Y. Wang for access to her lab and anaerobic glove box, and Dr. C. Hansel for providing synthetic Lp.

Supporting information for this article is available on the WWW under http://dx.doi.org/10.1002/anie.201406131.

further steps, the tooth interior is filled with a softer mineral or mixture of minerals. The minerals used in the core, and architectural details such as layers of lepidocrocite [Lp, γ-FeO(OH)] are characteristics of the chiton species. Overall, the architecture of a hard, abrasion-resistant cap and a more compliant core is reminiscent of vertebrate teeth.

The functional architecture of the chiton tooth arises from a tightly controlled sequence of inorganic phase transformations with features that elude our synthetic capabilities. Unlike the biological process, where Fh is a precursor for a monolithic magnetite–organic nanocomposite with excellent mechanical properties, wet chemical synthesis results in nanodisperse magnetite powders. Furthermore, under physiological conditions and in the absence of strong ligands, only Fe^{II} is bioavailable. However, in the presence of oxygen at circumneutral pH values, Fe^{II} is rapidly oxidized to Fe^{III}. The latter immediately hydrolyzes to crystalline Lp or goethite [α-FeO(OH)], not metastable Fh, unless the reaction is performed under conditions of extreme pH values and/or rapid hydrolysis, far outside the physiological range.[4] Therefore, it is surprising that Fh precipitates during the formation of chiton teeth. Clearly, the organism manipulates the reaction environment in some fashion to enable Fh formation.

In other systems, acidic macromolecules are known to play a key role in controlling mineral nucleation, growth, and the transient stabilization of metastable amorphous calcium carbonate (ACC) and amorphous calcium phosphate (ACP).[9] Certain inorganic ions, such as phosphate in ACC, show similar activity.[10] Acidic macromolecules are likewise found in the organic matrix of chiton teeth and have been implicated in the unusual, selective decoration of chitin fibers with sodium or magnesium. The functional role of macromolecules in the chiton tooth remains poorly understood.[7,11] Phosphate concentrations in the mature cusp of chiton teeth are very low (< 0.1 atom % by electron-probe microanalysis); those in the forming tooth are not known and very hard to determine. Herein, we investigate the participation of the organic matrix and phosphate in the selective precipitation of metastable Fh under physiological conditions. Specifically, we probe the structure of the chemical environment of iron and its evolution during early tooth development.

Samples were cleaned to remove weakly bound iron,[12] all remaining iron present is insoluble (mineral) or strongly bound by the organic matrix. X-ray absorption near-edge structure (XANES) spectra show the evolution of the iron environment from Fh in stage 2 to magnetite in stage 4 (Figure 2).[13] However, we find that teeth in the "unmineralized" stage 1 not only show a distinct Fe *K*-edge, but also exhibit markedly different spectral features from later stages (Figure 2a,b), synthetic Fh, and magnetite (see Figure S1). Specifically, a broad post-edge shoulder decreases in intensity. A pre-edge feature (~7114 eV) increases in intensity, and the edge itself shifts to lower energy (Figure 2b). The latter shift is much more pronounced in stage 4 and is consistent with the partial reduction of Fe^{III} in Fh to Fe^{II} in magnetite.

The energy, splitting, and intensity distribution of the pre-edge feature are sensitive to spin state, oxidation state, geometry, and bridging ligation.[14] The intensity increase from stage 1 to stage 4 is consistent with a distorted octahedral coordination environment of high-spin Fe^{III} in Fh in stage 2 and the presence of tetrahedral Fe^{II} in magnetite in stage 4.[14b] In stage 1, the crystal field splitting (Figure 2c, $10Dq = 1.4$ eV) is larger than what is observed in synthetic Fh (Figure 2f, 0.95 eV), stage 2 (Figure 2d, 0.95 eV) and synthetic hydrated amorphous iron phosphate (1.2 eV). It is much closer to values of around 1.5 eV typically observed for octahedral, high-spin Fe^{III} complexes such as iron citrate and oxalate (Figure 2e and Table S1).[14a] A third component ($\approx$7116 eV) arising from Fe in the second shell is present in Fh and stage 2,[14b] but absent in stage 1, indicating that there is little or no sharing of ligands by iron octahedra. This is strong evidence that iron is present in low nuclearity complexes, not in a mineral with extensive bridging ligation (high nuclearity).[14a]

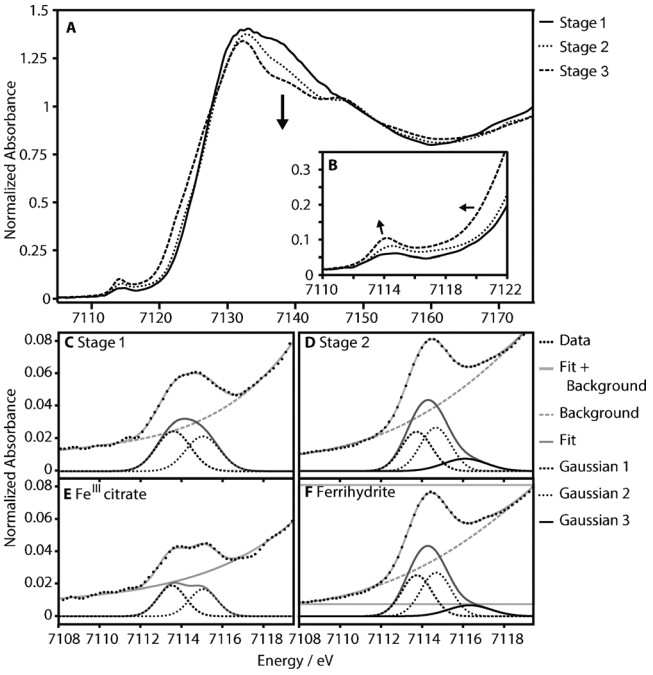

Figure 2. XANES spectra of chiton teeth and reference compounds. A) Normalized Fe *K*-edge spectra obtained from sections of *K. tunicata* radulae corresponding to stages 1, 2, and 4. Radulae of ten specimens were pooled for each sample. Arrow denotes a post-edge feature that decreases in intensity with increasing maturity of the teeth. B) In the pre-edge region, arrows highlight the increasing intensity of the pre-edge feature and the associated shift to lower energy of the pre-edge feature and the edge itself. C–F) Pre-edge fits for C) stage 1 teeth, D) stage 2 teeth, E) Fe^{III} citrate, and F) synthetic "2-line" Fh.

Extended X-ray absorption fine structure (EXAFS) analysis confirms this assessment. In *k*-space spectra, a pronounced beat pattern at 5 $Å^{-1}$ and 7.5 $Å^{-1}$, which is absent in stage 1 and Fe^{III} citrate, emerges in stage 2 and Fh, and increases in intensity in stage 4 and magnetite (Figure 3a and Figure S2). In real-space spectra, this corresponds to a strong increase in the second shell (Fe-Fe) scattering amplitude, indicating an increase in bridging ligation (Figure 3b).[15] In the same series, the amplitude from O in the first shell decreases, consistent with an increasingly distorted octahedral coordination environment.[15] Quantitative analysis was consistent with these qualitative results (see Figure S2 and

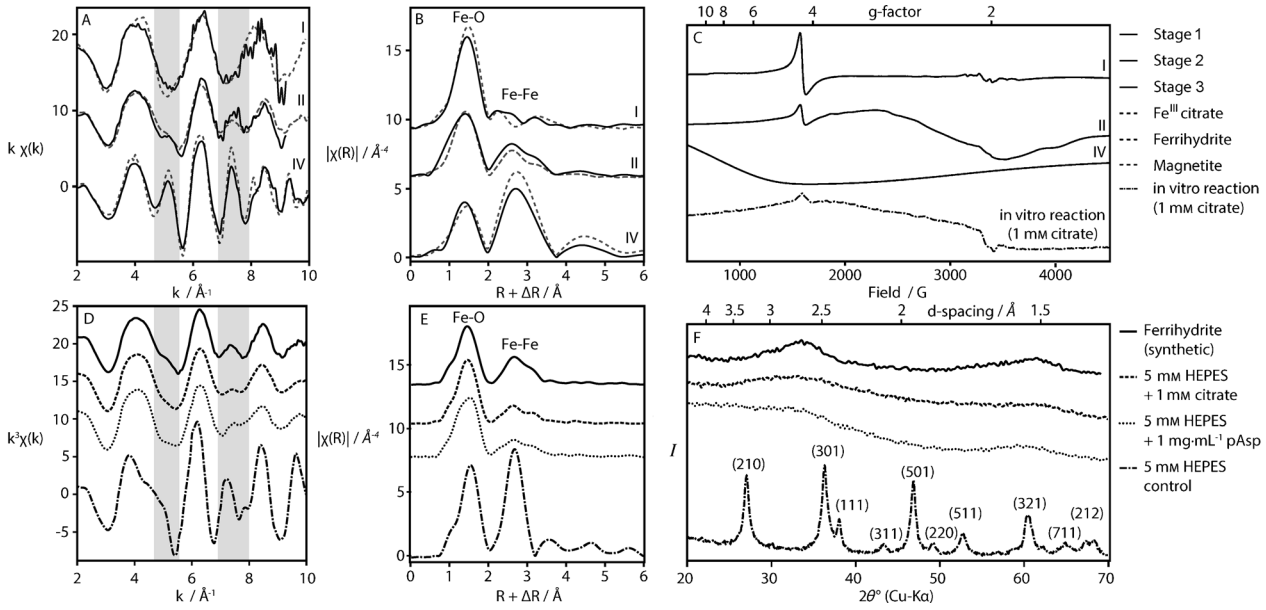

Figure 3. Fe *K*-edge EXAFS, *X*-band EPR, and XRD of chiton teeth, reference compounds, and in vitro reaction products. Radula sections were pooled from 10 animals for EXAFS and 2 animals for EPR. A) *k*-space and B) real-space EXAFS spectra (solid lines), overlaid with the corresponding reference compound (dashed lines), that is, Fe^{III} citrate for stage 1, Fh for stage 2, and magnetite for stage 4. *k*-space spectral components originating from second-shell Fe-Fe scattering at 5 $Å^{-1}$ and 7.5 $Å^{-1}$ are highlighted in gray. Real space Fe-O and Fe-Fe scattering shells are labeled over the corresponding peaks. C) In EPR spectra, a narrow resonance at $g \approx 4.2$ (dashed line) in stage 1 and 2 corresponds to high-spin mononuclear Fe^{III}. Note the similarity of the spectra of stage 2 teeth and Fh precipitated in vitro in the presence of citrate as a model ligand. D) Representative *k*-space EXAFS, E) real space EXAFS, and F) powder X-ray diffraction (XRD) patterns of in vitro reaction products (100 mM HEPES buffer, pH 7.2, and ligands, see Table 1). Spectra are offset vertically for clarity.

Table S2 in the Supporting Information). We conclude that iron in stage 1 is present in octahedral complexes with little or no bridging ligands.

Electron paramagnetic resonance (EPR) spectroscopy was chosen as a complementary technique for its sensitivity to oxidation state and local environment of paramagnetic Fe^{III}.[16] EPR spectra of stage 1 teeth exhibit a narrow resonance at $g \approx 4.2$, consistent with a mononuclear high-spin Fe^{III} iron complex (Figure 3c). Note that the peak-to-peak line width (56 G) is approximately 2.2 times broader than the corresponding resonance in the spectrum of the soluble mononuclear complex $[Fe(EDTA)]^-$ (Figure S3). This is consistent with iron present primarily in mononuclear complexes with organic matrix molecules in a variety of slightly different geometries but not iron oxide/phosphate minerals. The resonance at $g \approx 4.2$ is significantly weaker in stage 2, where a broad resonance at a lower *g*-factor dominates the spectrum, consistent with the presence of mineralized iron oxyhydroxides such as Fh (Figure S3). In stage 4, the only feature present is an extremely broad resonance typical for magnetite, observed previously in mature chiton teeth.[17]

Having confirmed that in stage 1, Fe^{III} occurs predominantly in low-nuclearity complexes, we probed the possible functional role of such complexes under simulated physiological conditions in vitro (Figure 3d–f, Table 1, and Figure S4). When an oxygen-free solution of $FeCl_2$ in HEPES buffer without further additives was oxidized in air, orange, crystalline Lp precipitated. Lp was also the predominant product (by linear combination fitting of EXAFS spectra)

Table 1: In vitro reaction conditions and yields determined by linear combination fitting of EXAFS spectra.

Ligand	Concentration [mM]			Fraction [%]		
	Ligand	HEPES	Fe^{2+}	Lp	Fh	[Fe^{III}]
buffer	0	100	5	**98**	0	2[a]
BSA	1.5[b]	100	5	**84**	16	1[a]
chitin	–	5	100	**83**	12	5[a]
citrate	1	100	5	0	**82**	18
citrate	5	100	5	3[a]	**52**	46
pAsp	1.8[c]	100	5	20	**71**	9
pAsp	8.8[c]	100	5	0	**69**	31

[a] Values of $\leq 5\%$ may not be significant. [b] Ligand concentration based on 98 Glu/Asp per BSA. [c] Equivalent Asp concentration in pAsp (2–11 kg mol^{-1}) solution. Fits are shown in Figure S5. [Fe^{III}] = Fe^{III} complex. Entries in bold face font mark the predominant fraction.

when bovine serum albumin (BSA), a moderately acidic protein with substantial metal-binding capacity (p*I* = 5.7, 98 Glu/Asp residues), was added, and in hydrogels formed from reconstituted chitin in buffer. However, when either the chelator citric acid, or poly(aspartic acid) (pAsp), a model compound for highly acidic proteins, were added, stable colloidal mixtures of "2-line" Fh and iron complexes formed instead (Figure 3d–f, Table 1, and Figure S4). In EPR spectra of colloids formed in the presence of citric acid, a narrow resonance at $g \approx 4.2$ reveals the presence of low-nuclearity, high-spin Fe^{III} complexes in addition to Fh (Figure 3c); the resulting spectra are quite similar to those of stage 2 chiton teeth. Powder X-ray diffraction patterns (Figure 3f) are consistent with Fh formed in the presence of acidic ligands.[18]

These results confirm the suppression of Lp formation in the presence of ligands.[19] They further indicate that highly acidic macromolecules in the chiton tooth scaffold may be essential for selective precipitation of Fh. A caveat is that we assume here that precipitation is initiated by oxidation of Fe^{II} after secretion into the scaffold. Our findings further expand the role of acidic macromolecules in the scaffold of the chiton tooth that were recently suggested to selectively bind sodium and magnesium.[2a] Iron carboxylate complexes with low nuclearity appear to have an integral role in this mechanism that may also be active in ferritin and magnetosomes.[6,20,21] In contrast to magnetite synthesis via a phosphate-rich precursor in magnetotactic bacteria, phosphate does not appear to be involved in Fh synthesis in the chiton.[2a,21] The formation of stable colloids of Fh in the presence of pAsp suggests that chitin fibers decorated with Fe^{III} complexes may act as heterogeneous nucleators of Fh, but at the same time limit growth to small nanoparticles.[22] Preventing aggregation and thus maintaining a high surface area may be important to ensure subsequent formation of monolithic magnetite in the chiton tooth. Patterning of the chitin tooth scaffold with acidic macromolecules might be a straightforward way for chitons to achieve the remarkable degree of spatial control over the mineral polymorphs within their teeth, for instance the deposition of a thin layer of Lp below the magnetite cusp in some species.[1a] This approach is conceptually related to the patterning of the macromolecules in the mollusk shell, the periodontal ligament,[23] or the action of the protein Starmaker in the zebrafish.[24] In a similar fashion, the organism could create graded interfaces, which are important for the mechanical function of human teeth.[25] Given that chiton teeth are the hardest and most wear-resistant biominerals, being able to expropriate this approach using straightforward chemistry has profound implications for the synthesis of bioinspired materials.

Received: June 11, 2014
Revised: July 11, 2014
Published online: September 2, 2014

Keywords: biomineralization · ferrihydrite · iron oxides · metastable compounds · organic matrix

[1] a) H. A. Lowenstam, S. Weiner, *On biomineralization*, Oxford University Press, Oxford, **1989**; b) J. C. Weaver, Q. Wang, A. Miserez, A. Tantuccio, R. Stromberg, K. N. Bozhilov, P. Maxwell, R. Nay, S. T. Heier, E. DiMasi, D. Kisailus, *Mater. Today* **2010**, *13*, 42 – 52.

[2] a) L. M. Gordon, D. Joester, *Nature* **2011**, *469*, 194 – 197; b) L. Evans, D. Macey, J. Webb, *Mar. Biol.* **1991**, *109*, 281 – 286.

[3] a) Q. Wang, M. Nemoto, D. Li, J. C. Weaver, B. Weden, J. Stegemeier, K. N. Bozhilov, L. R. Wood, G. W. Milliron, C. S. Kim, D. Kisailus, *Adv. Funct. Mater.* **2013**, *23*, 2908 – 2917; b) K.-S. Kim, D. Macey, J. Webb, S. Mann, *Proc. R. Soc. London Ser. B* **1989**, *237*, 335 – 346; c) C. M. Hansel, S. G. Benner, S. Fendorf, *Environ. Sci. Technol.* **2005**, *39*, 7147 – 7153.

[4] R. M. Cornell, U. Schwertmann, *The iron oxides*: *structure*, *properties*, *reactions*, *occurrences and uses*, Wiley, Hoboken, **2003**.

[5] a) F. M. Michel, V. Barrón, J. Torrent, M. P. Morales, C. J. Serna, J.-F. Boily, Q. Liu, A. Ambrosini, A. C. Cismasu, G. E. Brown, *Proc. Natl. Acad. Sci. USA* **2010**, *107*, 2787 – 2792; b) J. Baumgartner, A. Dey, P. H. Bomans, C. Le Coadou, P. Fratzl, N. A. Sommerdijk, D. Faivre, *Nat. Mater.* **2013**, *12*, 310 – 314; c) D. Li, M. H. Nielsen, J. R. Lee, C. Frandsen, J. F. Banfield, J. J. De Yoreo, *Science* **2012**, *336*, 1014 – 1018; d) J. F. Banfield, S. A. Welch, H. Zhang, T. T. Ebert, R. L. Penn, *Science* **2000**, *289*, 751 – 754.

[6] L. P. Rosenberg, N. D. Chasteen in *The Biochemistry and Physiology of Iron* (Eds.: P. Saltman, J. Hegenauer), Vol. 1, 405 – 407. Elsevier North Holland, Amsterdam, **1982**.

[7] L. R. Brooker, J. A. Shaw, Seto J. Advanced Topics in Biomineralization. InTech **2012**, 65 – 84.

[8] Q. Wang, M. Nemoto, D. Li, J. C. Weaver, B. Weden, J. Stegemeier, K. N. Bozhilov, L. R. Wood, G. W. Milliron, C. S. Kim, E. DiMasi, D. Kisailus, *Adv. Funct. Mater.* **2013**, *23*, 2908 – 2917.

[9] S. Mann, *Biomineralization: principles and concepts in bioinorganic materials chemistry*, *Vol. 5*, Oxford University Press, Oxford, **2001**.

[10] a) S. Weiner, L. Addadi, *Annu. Rev. Mater. Res.* **2011**, *41*, 21 – 40; b) J. Mahamid, A. Sharir, L. Addadi, S. Weiner, *Proc. Natl. Acad. Sci. USA* **2008**, *105*, 12748 – 12753.

[11] M. Nemoto, Q. Wang, D. Li, S. Pan, T. Matsunaga, D. Kisailus, *Proteomics* **2012**, *12*, 2890 – 2894.

[12] J. A. Shaw, D. J. Macey, P. L. Clode, L. R. Brooker, R. I. Webb, E. J. Stockdale, R. M. Binks, *Am. Malacol. Bull.* **2008**, *25*, 35 – 41.

[13] C. Numako, I. Nakai, *J. Phys. IV* **1997**, *7*, 2 – 2.

[14] a) T. E. Westre, P. Kennepohl, J. G. DeWitt, B. Hedman, K. O. Hodgson, E. I. Solomon, *J. Am. Chem. Soc.* **1997**, *119*, 6297 – 6314; b) M. Wilke, F. Farges, P.-E. Petit, G. E. Brown, F. Martin, *Am. Mineral.* **2001**, *86*, 714 – 730.

[15] C. Mikutta, J. Frommer, A. Voegelin, R. Kaegi, R. Kretzschmar, *Geochim. Cosmochim. Acta* **2010**, *74*, 5574 – 5592.

[16] F. Bou-Abdallah, N. D. Chasteen, *JBIC J. Biol. Inorg. Chem.* **2008**, *13*, 15 – 24.

[17] B. P. Weiss, S. Sam Kim, J. L. Kirschvink, R. E. Kopp, M. Sankaran, A. Kobayashi, A. Komeili, *Earth Planet. Sci. Lett.* **2004**, *224*, 73 – 89.

[18] K. Eusterhues, F. E. Wagner, W. Häusler, M. Hanzlik, H. Knicker, K. U. Totsche, I. Kögel-Knabner, U. Schwertmann, *Environ. Sci. Technol.* **2008**, *42*, 7891 – 7897.

[19] G. Krishnamurti, P. Huang, *Clays Clay Miner.* **1991**, *39*, 28 – 34.

[20] M. I. Siponen, P. Legrand, M. Widdrat, S. R. Jones, W.-J. Zhang, M. C. Chang, D. Faivre, P. Arnoux, D. Pignol, *Nature* **2013**, *502*, 681 – 684.

[21] J. Baumgartner, G. Morin, N. Menguy, T. P. Gonzalez, M. Widdrat, J. Cosmidis, D. Faivre, *Proc. Natl. Acad. Sci. USA* **2013**, *110*, 14883 – 14888.

[22] A. Navrotsky, L. Mazeina, J. Majzlan, *Science* **2008**, *319*, 1635 – 1638.

[23] a) L. Addadi, D. Joester, F. Nudelman, S. Weiner, *Chem. Eur. J.* **2006**, *12*, 980 – 987; b) A. J. Lausch, B. D. Quan, J. W. Miklas, E. D. Sone, *Adv. Funct. Mater.* **2013**, *23*, 4906 – 4912.

[24] C. Söllner, M. Burghammer, E. Busch-Nentwich, J. Berger, H. Schwarz, C. Riekel, T. Nicolson, *Science* **2003**, *302*, 282 – 286.

[25] P. Zaslansky, A. A. Friesem, S. Weiner, *J. Struct. Biol.* **2006**, *153*, 188 – 199.

